JOURNAL OF AGRICULTURAL AND FOOD CHEMISTRY

J. Agric. Food Chem. **2008,** *56,* 10557–10566 **10557**

Crystal and Molecular Structure of Piceatannol; Scavenging Features of Resveratrol and Piceatannol on Hydroxyl and Peroxyl Radicals and Docking with Transthyretin

MIRIAM ROSSI,*[,†,‡] FRANCESCO CARUSO,[‡,§] CRISTIAN OPAZO,[||] AND JUSTIN SALCICCIOLI[†]

Department of Chemistry, Vassar College, Poughkeepsie, New York 12604-0484, Istituto di Chimica Biomolecolare, Consiglio Nazionale delle Ricerche (CNR), c/o University of Rome, Istituto Chimico, Piazzale Aldo Moro 5, 00185, Rome, Italy, and Academic Computing Services CIS, Vassar College, Poughkeepsie, New York 12604-0748

The mechanism by which the naturally occurring polyphenolic compounds resveratrol (RES), $C_{14}H_{12}O_3$, and its metabolite piceatannol (PIC), $C_{14}H_{12}O_4$, scavenge free radicals is studied using experimental and density functional theory (DFT) methods. PIC's crystal structure shows a strong intermolecular hydrogen bond network, which, through a concerted motion of the hydroxyl hydrogen atoms, can produce a second hydrogen bond chain. This reorganization offers a low-energy pathway for the transfer of hydrogen atoms and is a contributing factor to PIC's biological activity. Additionally, DFT calculations describing the entire reaction mechanism of RES, PIC, and 3,3′,4′,5,5′-pentahydroxystilbene with hydroxyl and peroxyl radicals agree with experimental results, showing that increased hydroxylation aids in scavenging activity. PIC is more efficient than RES because (i) by sharing its 3′-OH hydrogen atom with its adjacent neighbor, O-4′, the abstraction and transfer of the 4′-H atom to the free radical becomes easier and (ii) the resulting PIC semiquinone radical is more stable. As a result of the reaction with $OH^{\bullet}$, both RES and PIC form water; with the peroxyl radical, both RES and PIC form hydrogen peroxide. Also, docking of PIC onto the protein transthyretin suggests better performance than RES and confirms its possible application in neurodegenerative conditions such as Alzheimer's disease.

KEYWORDS: Piceatannol; antioxidant; free radical scavenger; crystal structure; DFT; transthyretin

INTRODUCTION

Over the years, an increasing amount of research has focused on the potential health benefits of naturally occurring compounds in fruits and vegetables due to their high levels of biological activity and low toxicity. One of the most closely studied compounds, *trans*-3,4′,5-trihydroxystilbene, resveratrol (RES), found in red wine, grape products, berries, and peanuts, has demonstrated a wide variety of positive biological effects (*1, 2*). The activity of RES and other polyhydroxylated stilbenes is associated with the location and number of phenolic hydroxyl groups, the subsequent hydrogen-bonding capability, and the generation of stable resonance structures in the presence of oxidative electrophilic species (*3*). Therefore, structural analogues of RES are also of significant interest; piceatannol (3′,4′,3,5- tetrahydroxystilbene; PIC) (**Scheme 1**), differs from RES in that it possesses an extra hydroxyl group (labeled O2 in **Figure 1**) adjacent to the active 4′-OH of RES. PIC is present in minute quantities in peanuts (*4*), *Euphorbia lagascae* (*5*), *Vaccinium* berries (*6*), grapes (*7*), and in many species containing RES (*8*): *Polygonum cuspidatum*, *Vitis thunbergii*, and *Ampelopsis brevipedunculata*. In humans, PIC is produced as a major metabolite of RES by the cytochrome P450 enzymes (*9, 10*), CYP1B1and CYP1A2. It shows anti-inflammatory (*11, 12*) and antimicrobial effects (*13*). Evidence indicates that PIC activates protein heme oxygenase-1 (HO-1) (*14*) and is a potent tyrosine kinase inhibitor (*15*). It inhibits mitochondrial F type ATPase activity by targeting the F1 complex (*16*) and demonstrates higher levels of antioxidant activity than RES (*14*). PIC is successful against leukemia (*1, 17*) and induces apoptosis and antitumorigenic activities in several cell lines and animal models (*18*−*20*). Recently, after topical application in vivo but preceding UVB irradiation, it was shown to be effective against some effects of oxidative stress as measured by the production of lipid peroxides (*21*).

* To whom correspondence should be addressed. E-mail: rossi@vassar.edu.

† Department of Chemistry, Vassar College.

‡ Contributed equally to this work.

§ Consiglio Nazionale delle Ricerche (CNR).

|| Academic Computing Services CIS, Vassar College.

10.1021/jf801923j CCC: $40.75
Published on Web 10/30/2008

Scheme 1

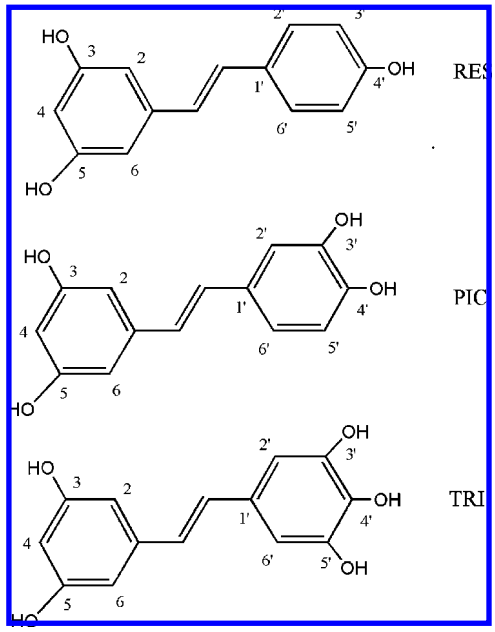

Experimentally, a number of studies have shown that *ortho*-dihydroxy groups are important for increased cytotoxic and antioxidant activity in vitro, although the mechanism for these processes remains unclear (*2, 22, 23*). Below, using a combination of single crystal X-ray diffraction and quantum mechanical ab initio methods, we examine the molecular structure of PIC in comparison to RES (*24*) to assess how the additional hydroxyl groups affect antioxidant activity toward hydroxyl and peroxyl radicals. We investigate PIC, RES, and 3,3′,4′,5,5′-pentahydroxystilbene (TRI).

In addition, many in vitro studies featuring naturally occurring polyphenols, including RES and PIC, are known to bind to tetrameric transthyretin (TTR) at the thyroxine binding site (*25*). In mammals, reptiles, and birds, TTR is the principal protein synthesized by the choroid plexus, a membrane belonging to the blood−brain barrier system, from where it is secreted into the cerebrospinal fluid (CSF) and in plasma serum; it is the major transporter for two endogenous small molecules: thyroxine (thyroid hormone T4) and retinol (jointly with retinol binding protein) at perpendicular binding sites. It exists as a tetramer (*26*) that sometimes, as a result of aging or inherited protein mutations, is able to disassociate into monomeric (*27*) amyloid fibrils. Small molecules bound to plasma proteins are retained for a long time, and thus, organisms are exposed to their effects for an extended period. They stabilize the TTR tetramer and prevent its disassociation to monomeric TTR amyloid fibrils that retain a secondary structure rich in β-sheets (*25, 28*−*31*).

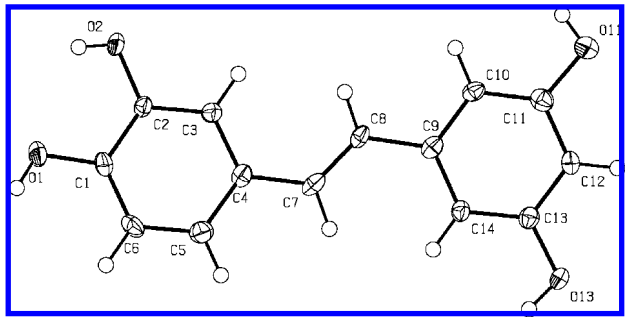

Figure 1. ORTEP drawing of PIC, $C_{14}H_{12}O_4$, showing anisotropic displacement ellipsoids.

Table 1. Crystal Data and Structure Refinement for PIC

empirical formula	$C_{14}H_{12}O_4$
formula weight	244.24
temperature	125(2) K
wavelength	0.71073 Å
crystal system, space group	monoclinic, *Pc*
unit cell dimensions	$a = 11.696(1)$ Å, $b = 4.9437(4)$ Å, $c = 10.1754(9)$ Å, $\beta = 107.648(1)°$
volume	560.65(9) Å^3
Z, calculated density	2, 1.447 mg/m^3
absorption coefficient	0.109 mm^{-1}
F(000)	256
crystal size	0.18 mm × 0.05 mm × 0.05 mm
θ range for data collection	1.83−29.39°
limiting indices	$-16 \le h \le 15$, $-6 \le k \le 6$, $-14 \le l \le 14$
reflections collected/unique	7380/1541 [*R*(int) = 0.0413]
completeness to $\theta = 29.39°$	99.6%
absorption correction	SADABS
max and min transmission	0.9947 and 0.9811
refinement method	full-matrix least-squares on F^2
data/restraints/parameters	1541/2/175
goodness-of-fit on F^2	1.056
R indices (all data)	*R*1 = 0.0601, *wR*2 = 0.1116
final *R* indices [$I > 2\sigma(I)$]	*R*1 = 0.0467, *wR*2 = 0.1057
largest diff. peak and hole	0.358 and −0.212 eÅ^{-3}

Also, both RES and PIC act on specific plasma membrane-binding sites in the rat brain that could increase TTR concentration and subsequently reduce amyloid β (Aβ) peptide toxicity (*32*).

In addition, TTR itself has been implicated as a protective agent in Alzheimer's disease, a neurodegenerative disorder characterized by the extracellular deposition of Aβ peptide and the formation of fibrils, since some CSF proteins such as TTR can bind with Aβ peptide and prevent Aβ from forming amyloid fibers (*33*). RES and PIC are known to bind at specific plasma membrane binding sites, which could increase the expression of TTR and perhaps lead to decreased Aβ peptide toxicity (*25*). RES and stilbene derivatives also show in vitro inhibition of Aβ polymerization and fibril formation by binding to Aβ peptide, although the molecular mechanism is not known (*30*). Consequently, to understand the interaction between PIC and TTR, a docking study of the two compounds was performed, and the result is also described below.

MATERIALS AND METHODS

X-ray Diffraction. Useful pale yellow crystals of PIC were grown in the cold (4 °C) from a methanol/water mixture. Crystallographic data were collected at low temperature using a Bruker SMART APEX II CCD X-ray diffractometer. The molecular structure was solved and refined using associated Bruker-SHELXTL software; details are in **Table 1** and the Supporting Information. H atoms were all clearly seen from the difference electron density map and were all refined except for the four hydroxyl Hs, which were constrained as riding on their oxygen atoms. Final *R*1 = 0.0467.

Theoretical Study. The structural features, transition state (TS), spin density, and energy parameters were calculated with theoretical methods using the density functional theory (DFT) program DMol3, implemented in Materials Studio 4.2 (PC platform) from Accelrys (*34*−*37*). The effect of water solvent was included using a COSMO algorithm (*38*). The local density setting was the general gradient approximation (GGA) (*39*) and the Becke exchange (BP) functional (*40*). A double numeric basis set with polarization functions (DNP) for an all-electron calculation was used (*37*). A related work showing the application of DMol3, not including solvent effect, for the hydroperoxyl radical action on RES has been recently published (*41*). Docking studies were performed with the CDOCKER (*42*) package in Discovery Studio 1.7 from Accelrys, and the active site radius was 10 Å in the conformer simulation for RES and PIC. The entire TTR protein was used to calculate the binding

Table 2. Hydrogen Bonds and Close Contact for PIC (Å and °)[a]

D−H···A	d(D−H)	d(H···A)	D(D···A)	<(DHA)>
O(1)−H(1)···O(2)#1	0.88(4)	1.95(4)	2.797(3)	162(4)
O(13)−H(13)···O(11)#2	0.86(4)	1.92(4)	2.782(3)	174(3)
O(2)−H(2)···O(13)#3	0.76(4)	2.00(4)	2.736(2)	163(4)
O(2)−H(2)···O(1)	0.76(4)	2.31(4)	2.725(3)	116(3)
O(1)···O(13)#3	0.88(4)		2.803(3)	
O(1)···O(11)#4			2.969(3)	

[a] Symmetry transformations used to generate equivalent atoms: #1, x, $-y+1$, $z+1/2$; #2, x, $-y$, $z+1/2$; #3, $x-1$, $y+1$, z; #4, $x-1$, $-y+1$, $-z+1/2$.

energies for the various ligand conformations, but for clarity, figures include only the monomer chain. The ligand minimization calculations included various conformations of RES and PIC. The first 10 conformations of RES did not have much variance in their binding energies with the protein (−78.0 to −78.9 kcal/mol), while the PIC conformations had significant variation (between −73.3 and −95.6 kcal/mol), and so, additional PIC conformations were studied; they indeed provided a larger range of energies reaching approximately −108 kcal/mol as shown in **Table 3**.

RESULTS AND DISCUSSION

Figure 1 shows the molecular structure and atom labels of PIC. Geometrical parameters confirm the stilbene character of the compound (Table S1 of the Supporting Information). The PIC molecules lie flat (as shown by the torsion angles involving the ethylene moiety and the two phenyl rings; Table S1 of the Supporting Information) with the long axis of the PIC molecules along the crystallographic *a*-axis; the molecules pack in a stepwise manner (Figure S1 of the Supporting Information) so that the hydrophilic hydroxyl groups O11 and O13 face another row of molecules oriented toward the hydroxyl groups O1 and O2, maximizing hydrogen bond interactions.

The directionality of hydrogen bonds makes them unique among intermolecular forces, and this feature can be exploited by antioxidants. Hydrogen-bonding reorganization offers a low-energy pathway for transfer of hydrogen atoms since reorientation of a hydrogen atom in one hydrogen bond induces a cooperative reorientation of the others in the nearby hydrogen-bonded molecules. Furthermore, unusual hydrogen-bonding interactions can indicate a metastable state of the molecule in the crystal. PIC's extensive hydrogen-bonding network listed in **Table 2** can best be seen down the *b*-axis and along the *c*-axis (**Figure 2**). In PIC, all of the hydrogen atom positions were observed experimentally in the difference Fourier electron density map. An investigation of the intermolecular hydrogen bond pattern in the crystal packing reveals that alternate sites for hydroxyl hydrogen atoms are possible and chemically favorable as they lead to formation of strong hydrogen bonds. For example, the observed position of H11 is clearly an average one since the hydrogen atom does not point toward any acceptor oxygen but, rather, is in between O13 and O1 from two different molecules and perpendicular to the triangular plane formed by O13, O1, and O11. Also, the anisotropic displacement ellipsoid on the hydroxyl oxygen atoms is clearly elongated in the direction corresponding to a second hydrogen bond position (**Figure 1**), implying movement of these oxygen atoms. As seen in **Table 2**, each of the hydroxyl oxygen atoms has at least two useful positions for hydrogen bonding, and fixing one hydrogen atom position to form a hydrogen bond causes all of the others to reorient to this hydrogen-bonding pattern. For example, from the experimental crystal structure shown in **Figure 2a**, if the position of H11 is chosen to form a hydrogen bond with O1 (O11−H11···O1), then an endless chain composed of hydrogen-bonding repeat units O1−H1···O2−H2···O13−H13···O11−H11 permeates the crystal structure. On the other hand, shifting the direction of H11 toward O13 to form O11−H11···O13 brings about a second hydrogen-bonding pattern. This mobility of the hydrogen bond chain is reminiscent of that observed earlier in the RES crystal structure (*24*) and suggests a possible mode of H transfer.

Table 3. Summary of ΔE (kcal/mol) and Distances (Å) for PIC, RES, and TRI Scavenging of $O_2^{\bullet -}$ and $OH^{\bullet}$ Radicals (Sc = Scavenger)

	$O_2^{\bullet -}$		$OH^{\bullet}$	
	ΔE	distances	ΔE	distances
RES-4′	−133.8	Sc-O4′--H, Rad-O--H 1.400, 1.099 partial	−166.7	Sc-O4′--H, Rad-O−H 1.765, 0.095 (**Figure 3b**)
	−162.7	Sc-O4′--H, Rad-O--H 1.616, 1.018 whole		
RES-5		Sc-O5--H, Rad-O--H 1.039, 1.549 partial		
PIC-4′	−20.5	Sc-O4′--H, Rad-O--H 1.547, 1.032 partial	−54.0	Sc-O4′--H, Rad-O--H 1.792, 0.992 (**Figure 8b**)
	−95.7	Sc-O4′--H, Rad-O--H 1.715, 1.002 whole		
PIC-5		Sc-O5--H, Rad-O--H 1.052, 1.478 partial		
	11.4	Sc-O4′--H, Rad-O--H 1.076, 1.418 whole		
TRI		Sc-O4--H, Rad-O−H 1.592, 1.020 partial		Sc-O4--H, Rad-O−H 2.028, 0.977 (**Figure 13**)

Other intermolecular interactions include stacking of shifted PIC molecules at about 3.5 Å (Figure S1 of the Supporting Information). This is shorter than that observed in RES (*24*), hinting that PIC may be more efficient at electron transfer through the stacked molecules, and suggests that PIC may have better scavenger performance than RES. In summary, the short stacking distance along with the extensive hydrogen bond network are most likely strong contributing factors to PIC's biological activity.

Theoretical Analysis. Because PIC and RES show remarkable activity as free radical scavengers, we wish to clarify the nature of this mechanism in light of their structure. We analyze the interaction of both RES and PIC with the endogenously produced reactive hydroxyl ($OH^{\bullet}$) and peroxyl ($O_2^{\bullet -}$) radicals.

Hydroxyl Radical ($OH^{\bullet}$). To test RES's ability to scavenge the $OH^{\bullet}$ radical, RES 4′-hydroxyl hydrogen and $OH^{\bullet}$ were placed initially at van der Waals distance, and a subsequent geometry optimization was performed. The initial and converged (an energy minimum) structures are shown in **Figure 3** along with the spin density pattern of the converged state. Because of $OH^{\bullet}$ radical reactivity, there is abstraction of $H^{\bullet}$ from RES, followed by formation of a water molecule. This illustrates the scavenger effect: RES intercepts the reactive free radical ($OH^{\bullet}$) by forming a new, more stable, and biologically less damaging radical (RES-4′$^{\bullet}$) that has the unpaired electron delocalized through both aromatic rings (**Figure 3c**). However, the molecule of water and the newly formed RES-4′$^{\bullet}$ radical remain close in our calculation, (O---H = 1.765 Å, **Figure 3b**), and so, we consider this resulting species as intermediate I1. A new geometry optimization was performed having an initial state with O(RES-4′$^{\bullet}$)---H(H_2O) at van der Waals separation; results are shown in **Figure 4**.

ΔE (E = internal energy) between **Figures 3a** and **4a** is −36.2 kcal/mol, but the difference in energy for infinitely separated reactants and the intermediate I1 structure shown in **Figure 3b** is greater, −171.2 kcal/mol. It seems that the hydroxyl radical is capable of interacting with the scavenger

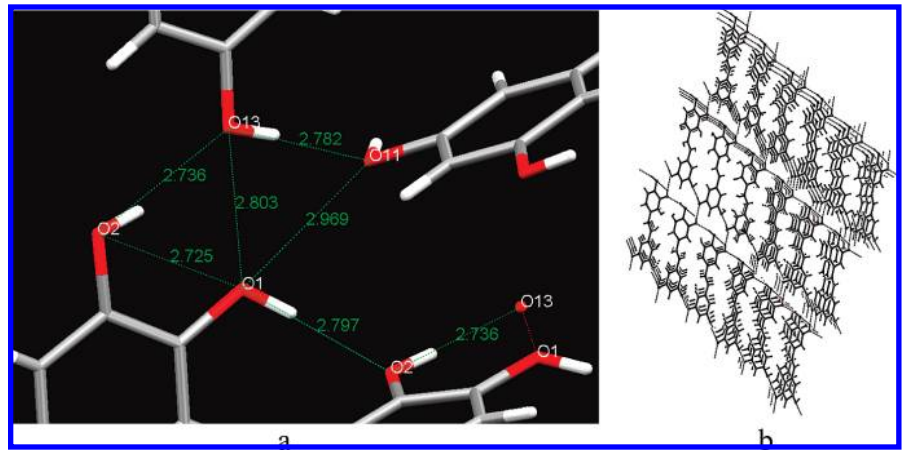

Figure 2. (**a**) Hydrogen bond distances, the O1 O11 is just about equal to van der Waals distance. The distances with esd's are also listed in **Table 2**; (**b**) packing H-bond pattern.

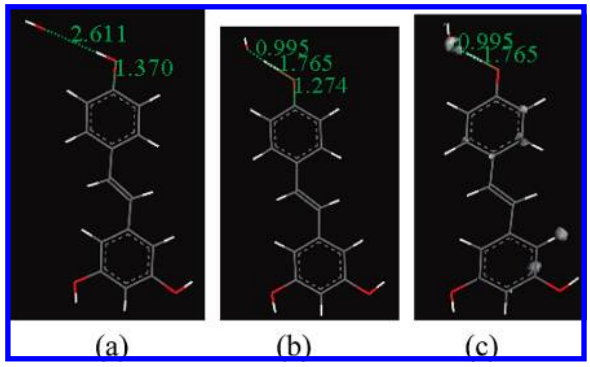

Figure 3. RES geometry optimization for the hydroxyl radical approach. Initial (**a**) and final (**b**) states plus the spin density (**c**) in the final state are shown (distances in Å).

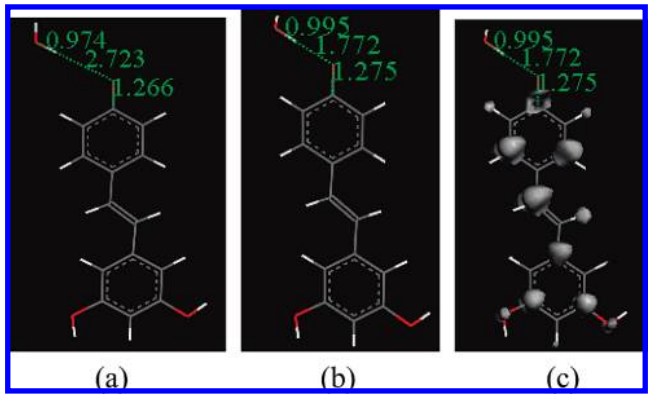

Figure 4. Interaction of RES-4′• radical with a molecule of water at van der Waals distance. Initial (**a**) and final (**b**) states plus spin density (**c**) of the final state are shown.

even at distances greater than van der Waals via transfer of its unpaired electron to neighboring molecules of water that eventually reach the scavenger. ΔE is equal to enthalpy at 0 K for conditions associated with no variation of volume and pressure ($\Delta H = \Delta E - P\Delta V - V\Delta P$) as in the studied reactions. In addition, ΔH is approximately equal to ΔG when ΔH is comparatively much larger than the term $T\Delta S$ at room T, as $\Delta G = \Delta H - T\Delta S$. This is generally true for small structural variation in going from reactants to products, as in the present case, where only an H atom is transferred from the scavenger to the radical. In this calculation, for completely separated reactants and products, ΔE is -166.7 kcal/mol ($\approx\Delta G$) and so, the scavenging of the OH• radical by RES is thermodynamically

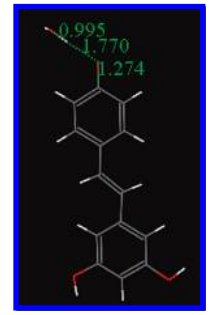

Figure 5. TS with relevant distances (Å) for the reaction between the H(4′-hydroxyl) of RES and the OH• radical.

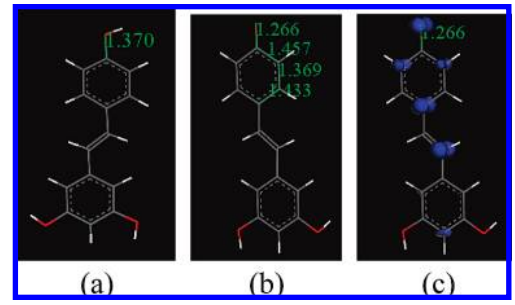

Figure 6. Converged structures of RES (**a**) and RES-4′ radical (**b**) plus spin density of the RES-4′ radical (**c**).

favored. This should be experimentally feasible if the configurations shown in part **b** of **Figures 3** and **4**, e.g., I1 and I2, can be connected through an energetically acceptable reaction pathway. Both intermediates were therefore considered as initial and final states for a TS search; ground-state energies differ slightly with I1 (**Figure 3b**) greater only by 0.4 kcal/mol. The obtained TS is characterized by a unique negative frequency. The TS was optimized and later confirmed using DMol3 standard procedures ($\nu = -26$ cm^{-1}). The activation energy connecting both structures is 0.07 kcal/mol; see **Figure 5**. Through geometry optimization of RES and its RES-4′• radical, shown in **Figure 6a**,**b**, it is seen that the TS, shown in **Figure 5**, is structurally closer to the RES-4′• radical than to RES, for example, C−O is 1.274 (TS), 1.266 (RES-4′• radical), and 1.370 Å (RES).

In summary, by donating its reactive 4′-H(hydroxyl) to form water, RES can assuage the strong OH• activity. This reaction is thermodynamically favored as its ΔE is negative (-166.7 kcal/mol), and because the TS involving both intermediates is characterized by a low barrier of energy (0.07 kcal/mol), it is

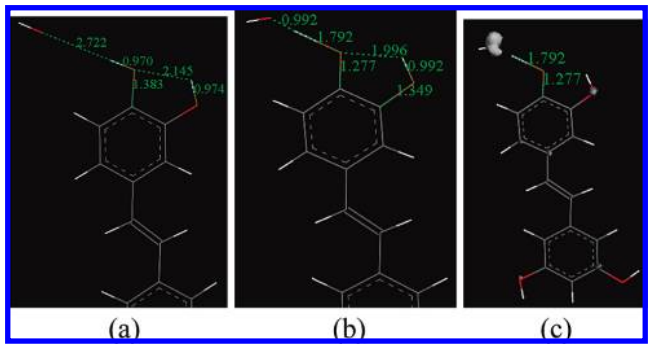

Figure 7. PIC geometry optimization for the hydroxyl radical approach toward 4′-hydrogen. Initial (**a**) and final state (**b**) plus the spin density (**c**) in the final state located on hydroxyl radical and 01 are shown.

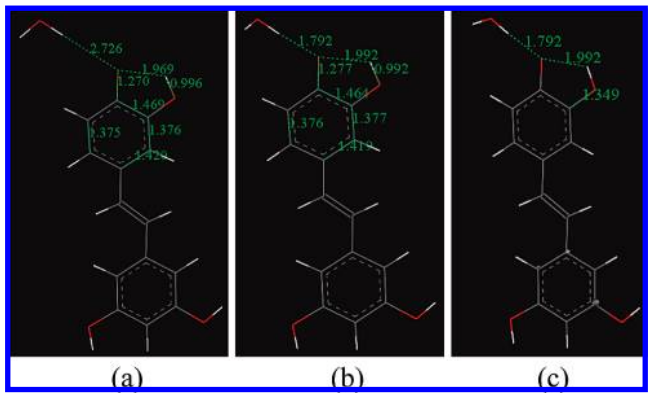

Figure 8. Interaction of PIC-4′′ radical and a molecule of water at van der Waals distance including initial (**a**) and final (**b**) states plus spin density (**c**) of the final state and located on C11 and C9 atoms.

likely to occur. The spin density of RES-4′′ radical is similar to the intermediate species obtained after $OH^{\bullet}$ approaches RES, demonstrating that the hydroxyl radical efficiently captures a hydrogen atom from RES, thereby making RES behave as a scavenger. In a related calculation, the abstraction of $H^{\bullet}$ (from α-tocopherol) by $OH^{\bullet}$ has been found to partially account for the whole scavenging reaction (*43*).

A similar study was calculated for PIC. Results shown in **Figures 7** and **8** are analogous to **Figures 3** and **4**, respectively. ΔE between parts **a** and **b** of **Figure 7** is −20.2 kcal/mol, while that between completely separated reagents and the intermediate structure depicted in **Figure 7b** is −62.9 kcal/mol. As with RES, the converged intermediate structure of **Figure 7b** has slightly lower energy than that of **Figure 8b** (0.2 kcal/mol), and a TS search was performed connecting them, but the linear synchronous transit path did not find a barrier, probably because it is even lower than that seen for RES. A comparison between RES and PIC geometry optimization paths shows that transfer of its 4′-$H^{\bullet}$ to the hydroxyl radical is more favored in PIC, as, at convergence, $H^{\bullet}$---$OH^{\bullet}$ separation is 0.995 (RES) and 0.992 Å (PIC), and scavenger release of $H^{\bullet}$ is enhanced (O4′---H distance of 1.756 and 1.792 Å, respectively). This is due to the 3′-OH sharing its H-3′ atom between O-4′ and O-3′, thus simplifying the abstraction and transfer of the 4′-H atom to the hydroxyl radical; this is consistent with X-ray structural results showing the strong intramolecular O2−H2···O1 hydrogen bond (**Figure 1** and **Table 2**). Also, the resulting PIC semiquinone radical is more stable. ΔE between completely separated reagents and products is −54.0 kcal/mol, and PIC scavenging of the hydroxyl radical is feasible.

Peroxyl Radical ($O_2^{\bullet -}$). As indicated by an experimental study performed by Murias (*23*), $O_2^{-\bullet}$ radical interaction with RES occurs via H-atom abstraction and proceeds in two steps

$$\mathrm{RES} + \mathrm{O_2}^{\bullet -} \rightarrow \mathrm{RES\text{-}4'^{\bullet}} + \mathrm{HO_2}^{-} \qquad \text{(R1)}$$

$$\mathrm{HO_2}^{-} + \mathrm{H}^{+} \rightarrow \mathrm{H_2O_2} \qquad \text{(R2)}$$

For step R1, RES-4′ hydroxyl hydrogen and $O_2^{\bullet -}$ were poised at van der Waals distance to perform a geometry optimization ($\Delta E = -133.8$ kcal/mol). As described earlier for the interaction with the hydroxyl radical, the two geometry-optimized products, RES-4′′ radical and HO_2^-, were poised at van der Waals separation to perform a geometry optimization, and these initial and final (converged) structures are depicted in **Figure 9**. ΔE between both intermediates is −0.9 kcal/mol, and a TS search protocol was set using the linear synchronous transit technique to find a unique imaginary frequency that was later optimized ($\nu = -543$ cm^{-1}) and whose structure is depicted in **Figure 10**. The E_a is 0.4 kcal/mol, and so, the reaction is kinetically allowed and feasible. For step R2, a geometry optimization for the structure shown in **Figure 9b** was performed after placing it at van der Waals distance from $[H_3O]^+$, a more realistic model than H^+; these initial state and converged final state structures are shown in **Figure 11**.

As indicated in **Table 3**, the whole reaction for scavenging the peroxyl radical has $\Delta E = -162.7$ kcal/mol, suggesting a strong scavenging capacity. An alternative option for step R2 may be to use a second molecule of RES as a potential H^+ donor for the formation of a molecule of viniferin as indicated in the literature for the diphenylpicryl hydrazyl (DPPH) radical scavenging (*44*) or in biological environment through COX-1 (*45*). We found a thermodynamically forbidden ΔE (36 kcal/mol) for this reaction.

The reactivity of PIC toward $O_2^{\bullet -}$ was similarly analyzed in two steps.

$$\mathrm{PIC} + \mathrm{O_2}^{\bullet -} \rightarrow \mathrm{PIC\text{-}4'^{\bullet}} + \mathrm{HO_2}^{-} \qquad \text{(P1)}$$

$$\mathrm{HO_2}^{-} + \mathrm{H}^{+} \rightarrow \mathrm{H_2O_2} \qquad \text{(P2)}$$

For step P1, the $O_2^{\bullet -}$ radical was poised at van der Waals distance from the PIC-4′ H(hydroxyl) to perform a geometry optimization: the 4′H left the aromatic moiety (H---O = 1.547 Å), and ΔE for this process is −20.5 kcal/mol. Step P2 was calculated theoretically by performing a geometry optimization on a system containing the previously converged structure from step P1, and $[H_3O]^+$ was poised so that one of its H atoms was located at van der Waals separation from the PIC 4′-O atom. **Figure 12** shows that the incoming hydronium cation induces further lengthening of the O---H separation (from 1.547 to 1.715 Å) and puts the H atom closer to the O(peroxyl) (from 1.032 to 1.002 Å); this suggests an enhanced capturing ability by PIC and the formation of hydrogen peroxide as the H(hydronium) approaches the peroxyl moiety (1.001 Å). The energetic change of this system indicates thermodynamic feasibility as the whole reaction has $\Delta E = -95.7$ kcal/mol. It is interesting that, when applied to RES, this process gave a different result as seen in Figure S2 of the Supporting Information; for example, the spin density associated with intermediate I1 in RES could not be transferred efficiently to the $O_2^{\bullet -}$ in our calculation, probably due to the barrier being slightly higher than in PIC. Nevertheless, as shown above, starting from intermediate I2 in RES, there is formation of hydrogen peroxide. This is another demonstration of the cooperative effect due to the existence of a hydroxyl moiety in position 3′ mentioned earlier. Comparison of **Figures**

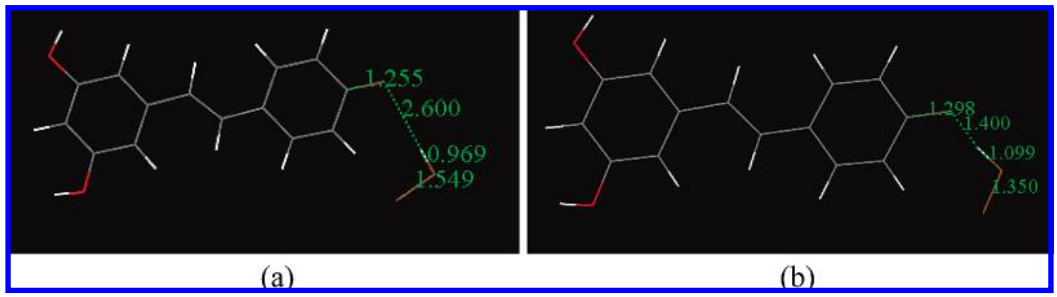

Figure 9. Initial and final state for van der Waals interaction between RES-4′• radical and HO_2^-.

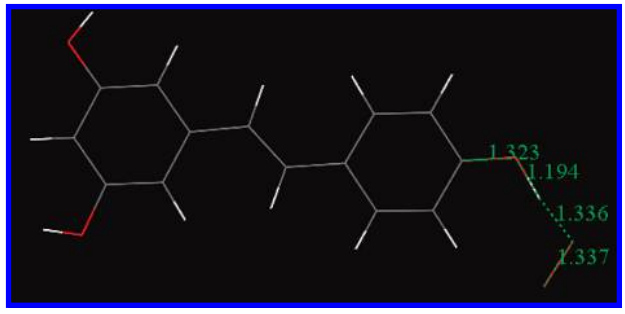

Figure 10. TS for RES-4′-OH scavenging the $O_2^{\bullet -}$ radical of reaction R1 ($E_{activation}$ = 0.4 kcal/mol, $\Delta E_{reaction}$ = −0.9 kcal/mol).

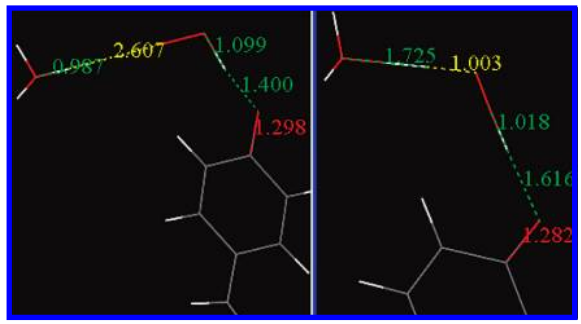

Figure 11. Initial and final state for a geometry optimization describing the interaction between the intermediate I2 and H_3O^+ to form H_2O_2 and water and the radical RES-4′•. Yellow numbers show the path of interaction between a hydronium H atom and one O(peroxyl) (range, 2.607−1.003 Å), while red numbers show an initial C−O bond length with some double bond character (1.298 Å) that is enhanced in the final state (1.282 Å); only part of RES is shown.

11 and **12** shows that PIC also is more effective than RES in forming a semiquinone radical as C4′---O bond lengths are 1.277 and 1.282 Å, respectively.

Therefore, the interaction of $O_2^{\bullet -}$ with PIC, followed theoretically, shows thermodynamic feasibility. DFT studies on the *ortho*-dihydroxyl moiety in catechin show that it forms an intermediate structure stabilized by a double H-bond upon interaction with radical species $CH_3O_2^{\bullet -}$ (*46*); we were not able to find such intermediate species for PIC---$O_2^{\bullet -}$. The presence of *ortho*-dihydroxyl groups in aromatic scavengers, besides implying more enhanced antioxidant activity, also involves formation of *ortho*-quinones as detected experimentally (*22*) and recently treated theoretically (*47*). We investigated a potential case for the PIC radical. Results from our calculations show positive ΔE for anionic conditions (**Scheme 2**, ΔE of 26.0 kcal/mol) and neutral (**Scheme 3**, ΔE of 19.2 kcal/mol), and so, such reactions are thermodynamically forbidden.

Previous studies (*24, 41*) revealed that RES *meta*-H(hydroxyl) atoms can also be considered potential scavengers, and so, an equivalent reaction was also checked for a PIC *meta*-H transfer.

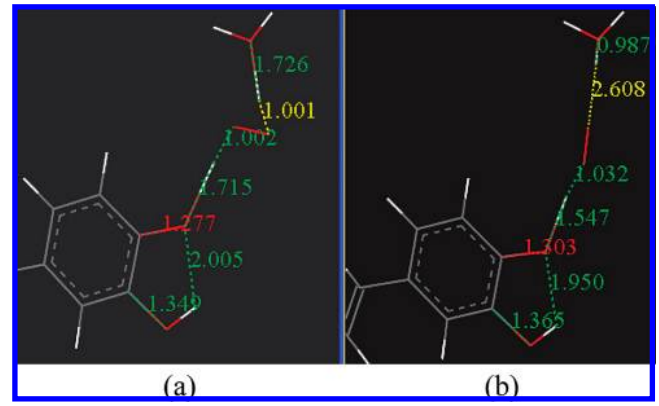

Figure 12. Final and initial state for a geometry optimization describing the interaction between the radical PIC-4′---$O_2^{\bullet -}$ and H_3O^+ to form H_2O_2, water, and the radical PIC-4′•. Yellow numbers show the path of interaction between a hydronium H atom and one O(peroxyl) (range, 2.608−1.001 Å), while red numbers show an initial C−O bond with some single character (1.303 Å) that shortens through the reaction pathway to become almost a double bond (1.277 Å); only part of PIC is shown.

Scheme 2

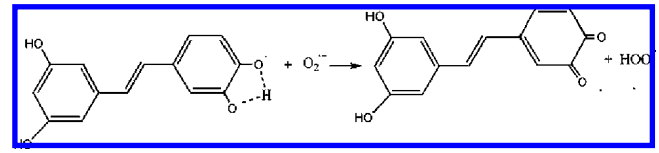

Scheme 3

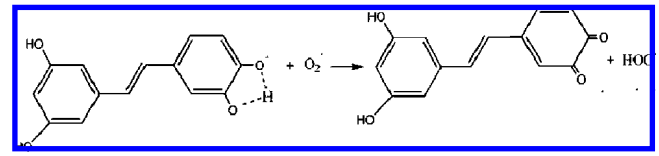

From the resulting ΔE = 11.4 kcal/mol for the whole process, **Table 3**, it is seen that PIC *meta*-H atoms cannot be transferred to the peroxyl radical; see Figure S3 of the Supporting Information. O(peroxyl) atoms are less able to establish bonding interactions with PIC-5 hydrogen atom than with the PIC-4′; that is, hydronium H---O(peroxyl) distances are 1.008 and 1.001 Å, respectively, whereas H---O(peroxyl) distances are 1.418 and 1.002 Å, respectively. Basically, during interaction of PIC-5 with $O_2^{\bullet -}$, its C−O5 (labeled C13−O13 in **Figure 1**) single bond character (1.340 Å) is conserved, whereas the 4′-radical (see **Figure 12**) C−O4′ has double bond character (1.277 Å). Moreover, the carbonyl-like calculated bond length C−O5 (1.281 Å) is longer than the corresponding C−O4′ (1.270 Å, **Figure 8a**) in the *para*-PIC-4′ radical, and so, the *meta* radical is less stable than the *para* radical. An alternative analysis regarding RES's *meta*-H transfer confirms PIC's results as shown in Figure S4 of the Supporting Information that depicts

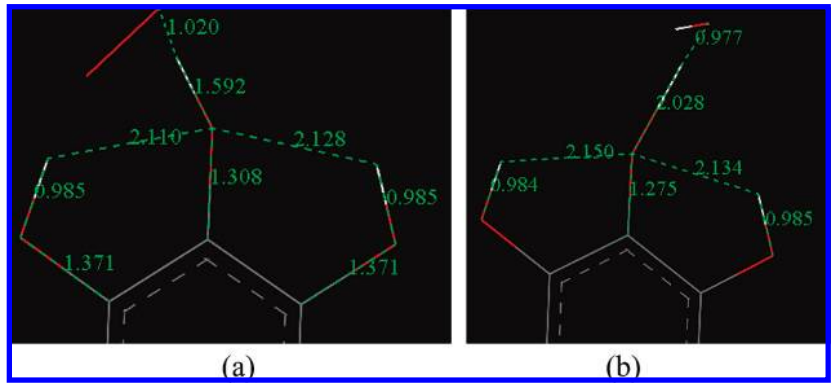

Figure 13. Converged structures after geometry optimization of TRI interaction with $O_2^{\bullet -}$ (**a**) and $OH^{\bullet}$ (**b**).

the $O_2^{\bullet -}$---RES-5 geometry optimization after $O_2^{\bullet -}$ attack. The H-5---O_2 distance (1.549 Å) is longer than H-4′---O_2 (1.099 Å, **Figure 11**), indicating that the *meta*-H(hydroxyl) is less likely to be transferred to the peroxyl radical. A closer approach of this *meta*-H-5 to $O_2^{\bullet -}$ while lengthening RES O-5----H and followed by geometry optimization were not effective in stabilizing the H within the O_2 bonding range. Moreover, performing a geometry optimization with the *meta*-H bound to O_2 (H---O_2 = 0.983 Å) and further lengthening RES-O-5---H separation (1.656 Å, Figure S5 of the Supporting Information), leads to the *meta*-H recovered by RES, again confirming the *meta*-OH to be less effective than the *para*-OH for scavenging the radical $O_2^{\bullet -}$.

As mentioned earlier, results from this theoretical analysis indicate that *ortho*-dihydroxyl aromatic moieties provide increased scavenger ability, in agreement with experiment (*22*). We therefore wanted to see if this finding could be improved upon with added hydroxylation. Indeed, in a recent study (*44*), several stilbene derivatives with varying number of hydroxyl groups were tested as free radical scavengers against DPPH; the amount of activity is RES < PIC < TRI, with radical inhibition of 55.1, 67.1, and 92.9%, respectively. In view of that, we studied theoretically the behavior of TRI; geometry optimization results for $OH^{\bullet}$ and partial $O_2^{\bullet -}$ scavenging are depicted in **Figure 13**. Comparing **Figure 13** with related pictures of PIC (**Figures 7a** and **12b**) and RES (**Figures 3b** and **11a**), it is seen that additional adjacent OH moieties on stilbenes are a positive feature for scavenging free radicals, in agreement with the literature (*44*). For $OH^{\bullet}$ scavenging, the number of hydroxyl groups is associated with a longer O(scavenger)---H(abstracted) separation [1.765 (RES), 1.792 (PIC), and 2.028 Å (TRI)] and a stronger O(free radical)−H(abstracted) bond formation [0.995 (RES), 0.0992 (PIC), and 0.977 Å (TRI)], whereas carbonyl stabilization within the scavenger is not substantially affected [1.274 (RES), 1.277 (PIC), and 1.275 Å (TRI)]. For $O_2^{\bullet -}$ scavenging (partial reaction), related results are O(scavenger)---H(abstracted) [separation of 1.400 (RES), 1.547 (PIC), and 1.592 Å (TRI)], while O(free radical)−H(abstracted) bond formation is 1.099 (RES), 1.032 (PIC), and 1.020 Å (TRI) and carbonyl stabilization within the scavenger is enhanced [1.282 (RES), 1.277 (PIC), and 1.275 Å (TRI)]. The greater damaging effect of $OH^{\bullet}$ as compared with $O_2^{\bullet -}$ is also estimated quantitatively from our calculations as the former more efficiently captures $H^{\bullet}$ from RES (0.995 Å) than $O_2^{\bullet -}$ (1.099 Å), from PIC (0.992 and 1.032 Å, respectively) and from TRI (0.997 and 1.020 Å, respectively).

Interactions with Proteins. PIC and RES are known to bind to and inhibit several proteins. X-ray structures of six protein−RES complexes are known (*28, 48*−*52*), while PIC is seen with the F1-ATPase (*52*). These investigations show the stilbene derivatives to be approximately planar and bound to the protein amino acids through hydrogen bonds to their hydroxyl groups, which are sometimes mediated by bound water molecules. In the present study, we use the X-ray structural results of the RES−human TTR crystal structure (*28*) (Figure S6 of the Supporting Information) and the PIC crystal structure for docking experiments to calculate PIC ability to interact with this important protein.

Table 4. Calculated Binding Energies of RES Analogues with TTR[a]

	kcal/mol		
	RES1	RES2	PIC
1	−78.5	−78.5	−73.3
2	−78.5	−78.5	−73.3
3	−78.4	−78.5	−73.3
4	−78.4	−78.5	−73.3
5	−78.0	−77.8	−84.0
6	−78.0	−77.8	−83.1
7	−78.0	−77.8	−83.1
8	−78.1	−78.3	−95.6
9	−78.1	−78.1	−84.9
10	−79.0*	−78.1	−84.8
11			−95.6
12			−108.0
13			−108.0
14			−108.0
15			−108.0
16			−108.0
17			−108.0
18			−108.1
19			−108.1
20			−108.1*

[a] Binding energies were calculated following CDOCKER, receptor−ligand minimization calculations. * indicates the conformations displayed in **Figures 14–16**. RES1 and RES2 indicate two different orientations of RES regarding H_2O154 molecules.

The inhibitory potential of both PIC and RES is related to the type, number, and location of phenolic functional groups and their ability to form hydrogen bonds with amino acid residues in the TTR thyroxine-binding site. The two columns shown in **Table 4** for RES refer to the spatial orientation of its 4′-H atom position. There are two symmetry-related water molecules (both labeled H_2O154), which correspond to the two halves of the protein near the 4′-OH group on RES. Because it is necessary to manually orient the hydrogen atoms to assess hydrogen bonding for the protein−ligand complex, the 4′-H atom was pointed toward each of the two H_2O154 molecules. For this reason, the minimization calculations were performed once with the 4′-H atom facing one of the water molecules (RES1) and another time with the 4′-H atom pointing toward the other water molecule (RES2). These RES results in the table do not differ very much from each other. Because the crystal

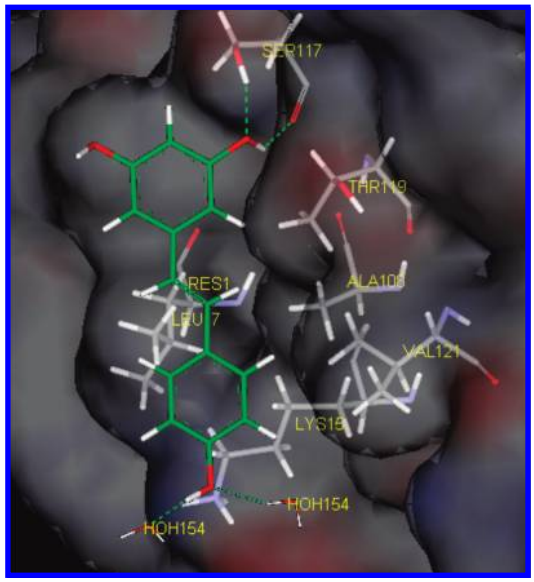

Figure 14. Structural view of the lowest energy TTR−RES complex. RES is sandwiched between two adjacent protein subunits to fill the central binding site channel. Only one dimeric half of the TTR structure is shown. TTR−RES hydrogen bonds are indicated (dashed green lines). The O3 hydroxyl group forms two hydrogen bonds with Ser117, while the 4′-hydroxyl group is bonded to both Lys15 residues by way of H_2O154 intermediates.

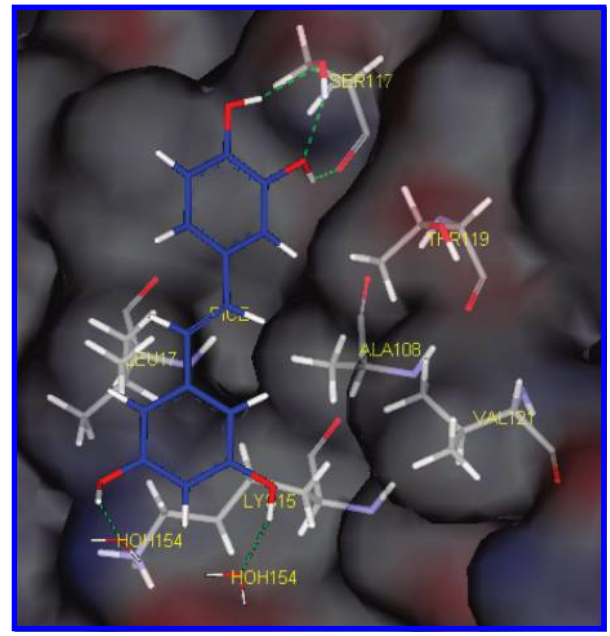

Figure 15. Structural view of the lowest energy TTR−PIC complex. The PIC ligand is sandwiched between two adjacent protein subunits to fill the central binding site channel. Only one dimeric half of the TTR structure is shown. TTR−PIC hydrogen bonds are indicated (dashed green lines). The O3 and O5 hydroxyl groups interact with Lys15 (not shown) of adjacent TTR subunits through intermediate hydrogen bonding with H_2O154.

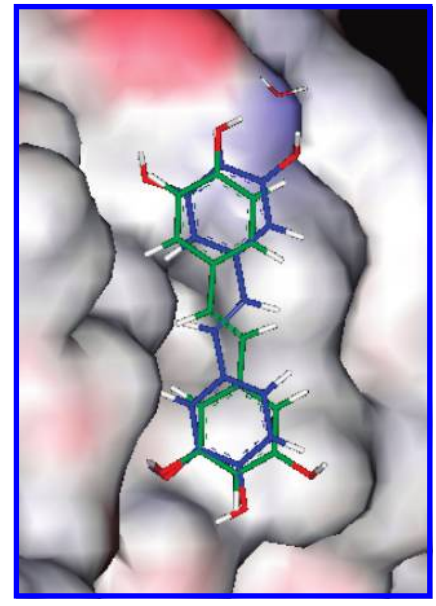

Figure 16. Structural overlay view of lowest energy TTR−RES complex as well as the lowest energy TTR−PIC complex. The TTR−RES complex has the RES 4′ (*para*) hydroxyl group oriented toward H_2O154, while the TTR−PICE complex has the PIC *para* hydroxyl group oriented away from the H_2O154. Hydrogen bonding and amino acid side chains are not shown.

structure describing PIC binding to TTR is not known, we applied the CDOCKER automatic procedure, which found PIC preferentially located in an inverted position with respect to RES; e.g., RES and PIC sit antiparallel (**Figure 16**). PIC interaction with H_2O154 molecules in the TTR active site is unique, and so, only one set of calculations is present in **Table 4**. The PIC inverted orientation allows it to maintain the hydrogen bonds to Lys15 side chains by the H_2O154 intermediates as seen with RES and also allows it to form three hydrogen bonds with Ser117, while the RES molecule has only two hydrogen bonds with Ser117. This additional hydrogen bonding of PIC with Ser117 accounts for its lower binding energy in comparison to RES. The TTR−PIC complex maintains a binding energy (approximately −108 kcal/mol), significantly lower than the TTR−RES complex (approximately −78 kcal/mol). It can be seen from **Figures 14**−**16** and **Table 4** that receptor−ligand minimization calculations for RES and PIC show binding energies more negative for the latter. This suggests that PIC can inhibit TTR amyloid fibril formation more strongly than RES.

Conclusions. The crystal structure determination shows that the PIC molecular structure is well-suited for a number of molecular reactions that make it biologically useful. Its hydroxyl groups allow for extensive and strong intermolecular and intramolecular (between adjacent hydroxyl groups) hydrogen bonding to occur throughout the system, permitting energetically favorable hydrogen atom transfer to take place, while stacking interactions of the planar stilbene system also may aid in electron transfer. The scavenging properties of RES and PIC are described at the molecular level using quantum mechanical methods. The ability of RES and PIC to scavenge free radicals is focused in this study on the transfer of the *para*-4′H(hydroxyl) atom. As demonstrated for reactions with $OH^{\bullet}$, *para*-H atom transfer is generally more efficient than *meta*. *Meta* positions also are not useful for scavenging $O_2^{\bullet -}$ as seen by positive ΔE for the reaction with PIC; RES structural features confirm this nonreactivity. PIC is more effective than RES at scavenging free radicals because its adjacent dihydroxyl moiety permits sharing of 3′-OH hydrogen atom between O3′ and O4′; this aids in the stabilization of the semiquinone 4′C═O formed upon 4′-OH hydrogen release. This is in agreement with increased scavenging activity for related di- and trihydroxyl derivatives and with PIC X-ray structural results, illustrating O···O 2.725(3) Å separation in the strong intramolecular hydrogen bond O(2)−H(2)···O(1). For $O_2^{\bullet -}$ scavenging, an approach of H^+

toward the PIC---O_2 radical entity is effective in completing the abstraction of $H^{\bullet}$ from PIC through formation of H_2O_2.

In summary, the 4′-OH group is a fundamental structural feature necessary for the radical scavenger activity in RES (*24*); the extra adjacent 3′-OH group in PIC increases the ability to capture the unpaired electron since the 3′-OH hydrogen atom is shared through a strong intramolecular hydrogen bond between O3′ and O4′. Subsequent resonance stabilization of the newly formed semiquinone PIC radical is the key to its success as a radical scavenger. Furthermore, results of protein docking studies of PIC with TTR suggest that PIC can inhibit TTR amyloid fibril formation more strongly than RES. This combination of X-ray crystallography and quantum mechanics is a powerful methodology for discovering the chemical behavior of biological molecules and produces results of increasing importance for structure−activity relationships in designing and recognizing medically valuable compounds.

ABBREVIATIONS USED

RES, resveratrol; PIC, piceatannol; DFT, density functional theory; TTR, transthyretin; TS, transition state; CSF, cerebrospinal fluid; Aβ, amyloid β; TRI, 3,4,5,3′,5′-pentahydroxy-*trans*-stilbene.

ACKNOWLEDGMENT

We thank the referees for their insightful comments.

Supporting Information Available: Stacking of PIC molecules (Figure S1); RES initial and final state for a geometry optimization describing the interaction between the intermediate radical RES-4′---$O_2^{\bullet -}$ and H_3O^+ to form H_2O_2, water, and the radical RES-4′′ (Figure S2); final and initial state for a geometry optimization describing the interaction between the radical PIC-5---$O_2^{\bullet -}$ and $[H_3O]^+$, only part of PIC shown (Figure S3); initial and final states for $O_2^{\bullet -}$ attack on a RES *meta* H(hydroxyl) (Figure S4); initial and final state for a geometry optimization applied to a supposed "captured" RES H(*meta*) by $O_2^{\bullet -}$ (Figure S5); TTR site cavity (Figure S6); and bond distances, bond angles, and torsion angles of PIC (Table S1). CIF file CCDC 706345 available at http://www.ccdc.cam.ac.uk/products/csd/request. This material is available free of charge via the Internet at http://pubs.acs.org.

LITERATURE CITED

(1) Saiko, P.; Szakmary, A.; Jaeger, W.; Szekeres, T. Resveratrol and its analogs: Defense against cancer, coronary disease and neurodegenerative maladies or just a fad. *Mutat. Res. Rev. Mutat. Res.* **2008**, *658*, 68–94.

(2) Baur, J. A.; Sinclair, D. A. Therapeutic potential of resveratrol: The in vivo evidence. *Nat. Rev. Drug Discovery* **2006**, *5*, 493–506.

(3) Stivala, L. A.; Savio, M.; Carafoli, F.; Perucca, P.; Bianchi, L.; Maga, G.; Forti, L.; Pagnoni, U. M.; Albini, A.; Prosperi, E.; Vannini, V. Specific structural determinants are responsible for the antioxidant activity and the cell cycle effects of resveratrol. *J. Biol. Chem.* **2001**, *276*, 22586–22594.

(4) Ku, K. L.; Chang, P. S.; Cheng, Y. C.; Lien, C. Y. Production of stilbenoids from the callus of arachis hypogaea: A novel source of the anticancer compound piceatannol. *J. Agric. Food Chem.* **2005**, *53*, 3877–3881.

(5) Ferrigni, N. R.; McLaughlin, J. L.; Powell, R. G.; Smith, C. R., Jr. Use of potato disk and brine shrimp bioassays to detect activity and isolate piceatannol as the antileukemic principle from the seeds of *Euphorbia lagascae*. *J. Nat. Prod.* **1984**, *47*, 347–352.

(6) Rimando, A. M.; Kalt, W.; Magee, J. B.; Dewey, J.; Ballington, J. R. Resveratrol, pterostilbene, and piceatannol in vaccinium berries. *J. Agric. Food Chem.* **2004**, *52*, 4713–4719.

(7) Bavaresco, L.; Fregoni, M.; Trevisan, M.; Mattivi, F.; Vrhovsek, U.; Falchetti, R. The occurrence of the stilbene piceatannol in grapes. *Vitis* **2002**, *41*, 133–136.

(8) Lin, L.; Lien, C.; Cheng, Y.; Ku, K. An effective sample preparation approach for screening the anticancer compound piceatannol using HPLC coupled with UV and fluorescence detection. *J. Chromatogr., B: Anal. Technol. Biomed. Life Sci.* **2007**, *853*, 175–182.

(9) Potter, G. A.; Patterson, L. H.; Wanogho, E.; Perry, P. J.; Butler, P. C.; Ijaz, T.; Ruparelia, K. C.; Lamb, J. H.; Farmer, P. B.; Stanley, L. A.; Burke, M. D. The cancer preventative agent resveratrol is converted to the anticancer agent piceatannol by the cytochrome P450 enzyme CYP1B1. *Br. J. Cancer* **2002**, *86*, 774–778.

(10) Piver, B.; Fer, M.; Vitrac, X.; Merillon, J.; Dreano, Y.; Berthou, F.; Lucas, D. Involvement of cytochrome P450 1A2 in the biotransformation of trans-resveratrol in human liver microsomes. *Biochem. Pharmacol.* **2004**, *68*, 773–782.

(11) Jin, C.; Moon, D.; Lee, K.; Kim, M.; Lee, J.; Choi, Y. H.; Park, Y.; Kim, G. Piceatannol attenuates lipopolysaccharide-induced NF-kB activation and NF-kB-related proinflammatory mediators in BV2 microglia. *Pharmacol. Res.* **2006**, *54*, 461–467.

(12) Richard, N.; Porath, D.; Radspieler, A.; Schwager, J. Effects of resveratrol, piceatannol, tri-acetoxystilbene, and genistein on the inflammatory response of human peripheral blood leukocytes. *Mol. Nutr. Food Res.* **2005**, *49*, 431–442.

(13) Docherty, J. J.; McEwen, H. A.; Sweet, T. J.; Bailey, E.; Booth, T. D. Resveratrol inhibition of propionibacterium acnes. *J. Antimicrob. Chemother.* **2007**, *59*, 1182–1184.

(14) Wung, B.-S.; Hsu, M.-C.; Wu, C.-C.; Hsieh, C.-W. Piceatannol upregulates endothelial heme oxygenase-1 expression via novel protein kinase C and tyrosine kinase pathways. *Pharmacol. Res.* **2006**, *53*, 113–122.

(15) Geahlen, R. L.; McLaughlin, J. L. Piceatannol (3,4,3′,5′-tetrahydroxy-trans-stilbene) is a naturally occurring protein-tyrosine kinase inhibitor. *Biochem. Biophys. Res. Commun.* **1989**, *165*, 241–245.

(16) Zheng, J.; Ramirez, V. D. Piceatannol, a stilbene phytochemical, inhibits mitochondrial F0F1-ATPase activity by targeting the F1 complex. *Biochem. Biophys. Res. Commun.* **1999**, *261*, 499–503.

(17) Ovesná, Z.; Kozics, K.; Bader, Y.; Saiko, P.; Handler, N.; Erker, T.; Szekeres, T. Antioxidant activity of resveratrol, piceatannol and 3,3′,4,4′,5,5′-hexahydroxy-trans-stilbene in three leukemia cell lines. *Oncol. Rep.* **2006**, *16*, 617–624.

(18) Larrosa, M.; Tomás-Barberán, F. A.; Espín, J. C. The grape and wine polyphenol piceatannol is a potent inducer of apoptosis in human SK-Mel-28 melanoma cells. *Eur. J. Nutr.* **2004**, *43*, 275–284.

(19) Wieder, T.; Prokop, A.; Bagci, B.; Essmann, F.; Bernicke, D.; Schulze-Osthoff, K.; Dorken, B.; Schmalz, H. G.; Daniel, P. T.; Henze, G. Piceatannol, a hydroxylated analog of the chemopreventive agent resveratrol, is a potent inducer of apoptosis in the lymphoma cell line BJAB and in primary, leukemic lymphoblasts. *Leukemia* **2001**, *15*, 1735–1742.

(20) Wolter, F.; Clausnitzer, A.; Akoglu, B.; Stein, J. The grape and wine polyphenol piceatannol is a potent inducer of apoptosis in human SK-Mel-28 melanoma cells. *J. Nutr.* **2002**, *132*, 298–302.

(21) Na, M.; Byung, S. M.; Bae, K. Protective effect of stilbenes on oxidative damage. *Nat. Prod. Sci.* **2007**, *13*, 369–372.

(22) Cai, Y.-J.; Wei, Q.-Y.; Fang, J.-G.; Yang, L.; Liu, Z.-L.; Wyche, J. H.; Han, Z. The 3,4-dihydroxyl groups are important for trans-resveratrol analogs to exhibit enhanced antioxidant and apoptotic activities. *Anticancer Res.* **2004**, *24*, 999–1002.

(23) Murias, M.; Jaeger, W.; Handler, N.; Erker, T. S.; Horvath, Z.; Szekeres, T.; Nohl, H.; Gille, L. Antioxidant, prooxidant and cytotoxic activity of hydroxylated resveratrol analogues: Structure-activity relationship. *Biochem. Pharmacol.* **2005**, *69*, 903–912.

(24) Caruso, F.; Tanski, J.; Villegas-Estrada, A.; Rossi, M. Structural basis for antioxidant activity of *trans*-resveratrol: Ab initio calculations and crystal and molecular structure. *J. Agric. Food Chem.* **2004**, *52*, 7279–7285.
(25) Almeida, M. R.; Gales, L.; Damas, A. M.; Cardoso, I.; Saraiva, M. J. Small transthyretin (TTR) ligands as possible therapeutic agents in TTR amyloidosis. *Curr. Drug Targets CNS Neurol. Dis.* **2005**, *4*, 587–596.
(26) Wojtczak, A.; Cody, V.; Luft, J. R.; Pangborn, W. Structures of human transthyretin complexed with thyroxine at 2.0 A resolution and 3′,5′-dinitro-N-acetyl-L-thyronine at 2.2 A resolution. *Acta Crystallogr.* **1996**, *D52*, 758–765.
(27) Pepys, M. B. Amyloidosis. *Annu. Rev. Med.* **2006**, *57*, 223–241.
(28) Klabunde, T.; Petrassi, H. M.; Oza, V. B.; Raman, P.; Kelly, J. W.; Sacchettini, J. C. Rational design of potent human transthyretin amyloid disease inhibitors. *Nat. Struct. Biol.* **2000**, *7*, 312–321.
(29) Porat, Y.; Abramowitz, A.; Gazit, E. Inhibition of amyloid fibril formation by polyphenols: Structural similarity and aromatic interactions as a common inhibition mechanism. *Chem. Biol. Drug Des.* **2006**, *67*, 27–37.
(30) Rivière, C.; Richard, T.; Quentin, L.; Krisa, S.; Mèrillon, J.-M.; Monti, J. P. Inhibitory activity of stilbenes on Alzheimer's β-amyloid fibrils in vitro. *Bioorg. Med. Chem.* **2007**, *15*, 1160–1167.
(31) Reixach, N.; Adamski-Werner, S. L.; Kelly, J. W.; Koziol, J.; Buxbaum, J. N. Cell based screening of inhibitors of transthyretin aggregation. *Biochem. Biophys. Res. Commun.* **2006**, *348*, 889–897.
(32) Han, Y.; Bastianetto, S.; Dumont, Y.; Quirion, R. Specific plasma membrane binding sites for polyphenols, including resveratrol, in the rat brain. *J. Pharmacol. Exp. Ther.* **2006**, *318*, 238–245.
(33) Costa, R.; Goncalves, A.; Saraiva, M. J.; Cardoso, I. Transthyretin binding to A-Beta peptide. Impact on A-Beta fibrillogenesis and toxicity. *FEBS Lett.* **2008**, *582*, 936–942.
(34) Accelrys Software, Inc. Telesis Court, Suite 100, San Diego, CA 92121.
(35) Delley, B. An all-electron numerical method for solving the local density functional for polyatomic molecules. *J. Chem. Phys.* **1990**, *92*, 508–517.
(36) Delley, B. From molecules to solids with the DMol3 approach. *J. Chem. Phys.* **2000**, *113*, 7756–7764.
(37) Delley, B. Fast calculation of electrostatics in crystals and large molecules. *J. Phys. Chem.* **1996**, *100*, 6107–6110.
(38) Klamt, A.; Schueuermann, G. COSMO: A new approach to dielectric screening in solvents with explicit expressions for the screening energy and its gradient. *J. Chem. Soc., Perkin Trans.* **1993**, *2*, 799–805.
(39) Perdew, J. P.; Chevary, J. A.; Vosko, S. H.; Jackson, K. A.; Pederson, M. R.; Singh, D. J.; Fiolhais, C. Atoms, molecules, solids, and surfaces: Applications of the generalized gradient approximation for exchange and correlation. *Phys. Rev. B: Condens. Matter Mater. Phys.* **1992**, *46*, 6671–6687.
(40) Becke, A. D. Density functional exchange energy approximation with correct asymptotic behavior. *Phys. Rev.* **1988**, *A38*, 3098–3100.
(41) Xu, S.; Wang, G.; Liu, H.; Wang, L.-J.; Wang, H.-F. A DMol3 study on the reaction between trans-resveratrol and hydroperoxyl radical: Dissimilarity of antioxidant activity among O-H groups of trans-resveratrol. *THEOCHEM* **2007**, *809*, 79–85.
(42) Wu, G.; Robertson, D. H.; Brooks, C. L., III.; Vieth, M. Detailed analysis of grid-based molecular docking: A case study of CDOCKER-A CHARMm-based MD docking algorithm. *J. Comput. Chem.* **2003**, *24*, 1549–1562.
(43) Navarrete, M.; Rangel, C.; Corchado, J. C.; Espinosa-Garcia, J. Trapping of the OH radical by α-tocopherol: A theoretical study. *J. Phys. Chem. A* **2005**, *109*, 4777–4784.
(44) Wang, M.; Jin, Y.; Ho, C.-T. Evaluation of resveratrol derivatives as potential antioxidants and identification of a reaction product of resveratrol and 2,2-diphenyl-1-picryhydrazyl radical. *J. Agric. Food Chem.* **1999**, *47*, 3974–3977.
(45) Szewczuk, L. M.; Lee, S. H.; Blair, I. A.; Penning, T. M. Viniferin formation by COX-1: Evidence for radical intermediates during co-oxidation of resveratrol. *J. Nat. Prod.* **2005**, *68*, 36–42.
(46) Tejero, I.; Gonzalez-García, N.; Gonzalez-Lafont, A.; Lluch, J. Tunneling in green tea: Understanding the antioxidant activity of catechol-containing compounds. A variational transition-state theory study. *J. Am. Chem. Soc.* **2007**, *129*, 5846–5854.
(47) Valgimigli, L.; Amorati, R.; Fumo, M. G.; DiLabio, G. A.; Pedulli, G. F.; Ingold, K. U.; Pratt, D. A. The unusual reaction of semiquinone radicals with molecular oxygen. *J. Org. Chem.* **2008**, *73*, 1830–1841.
(48) Buryanovskyy, L.; Fu, Y.; Boyd, M.; Ma, Y.; Hsieh, T. C.; Wu, J. M.; Zhang, Z. Crystal structure of quinone reductase 2 in complex with resveratrol. *Biochemistry* **2004**, *43*, 11417–11426.
(49) Austin, M. B.; Bowman, M. E.; Ferrer, J. L.; Schroder, J.; Noel, J. P. An aldol switch discovered in stilbene synthases mediates cyclization specificity of type III polyketide synthases. *Chem Biol.* **2004**, *11*, 1179–1194.
(50) Shomura, Y.; Torayama, I.; Suh, D. Y.; Xiang, T.; Kita, A.; Sankawa, U.; Miki, K. Crystal structure of stilbene synthase from Arachis hypogaea. *Proteins* **2005**, *60*, 803–806.
(51) Ferrer, J. L.; Jez, J. M.; Bowman, M. E.; Dixon, R. A.; Noel, J. P. Structure of chalcone synthase and the molecular basis of plant polyketide biosynthesis. *Nat. Struct. Biol.* **1999**, *6*, 775–784.
(52) Gledhill, J. R.; Montgomery, M. G.; Leslie, A. G.; Walker, J. E. Mechanism of inhibition of bovine F1-ATPase by resveratrol and related polyphenols. *Proc. Natl. Acad. Sci. U.S.A.* **2007**, *104*, 13632–13637.

Received for review June 23, 2008. Revised manuscript received September 4, 2008. Accepted September 18, 2008. X-ray facilities provided by the U.S. National Science Foundation (Grant #0521237), Vassar College (VC) Research Committee (M.R.), and VC URSI program (J.S.).

JF801923J